LOW AND HIGH STRAIN MACROBEHAVIOR OF GRAIN MASSES—THE EFFECT OF PARTICLE ECCENTRICITY

M. Aloufi, J. C. Santamarina

ABSTRACT. *High, medium, and low strain tests were conducted on green peas, white navy beans, and rice. These grains were selected to assess the effect of particle eccentricity on the mechanical behavior at different strain levels. Tests included interfacial ring shear, axisymmetric and true triaxials, simple shear, and wave propagation measurements. Index properties, microfabric analysis, and mechanical parameters are documented. Differences were found between the behavior of rice and the other two grains, which were explained as the result of the mechanical and geometrical characteristics of grains. Low-strain measurements reflected contact properties and fabric; both low and high strain properties were affected by stress history; major fabric changes occurred when shear strains exceed 3 to 10%; and extensive particle alignment took place after high shear deformation in elongated particles such as rice. The shear behavior at the interface with a rough surface was very similar for the three grains.* **Keywords.** *Grains, Particulate media, Microfabric, Wave velocity.*

The particulate nature of grains provides unique properties to the bulk medium. Hertz showed that two spheres made of linear elastic materials present a nonlinear force-displacement relationship when loaded with a force normal to the contact. Later, Mindlin showed that if an additional tangential force is added, and Coulomb's frictional behavior is assumed, an annular region around the periphery of the contact area slips unelastically (Richart et al., 1970; Mohsenin, 1970). It follows from Hertz' and Mindlin's theories that particulate media are inherently nonlinear and nonelastic. Another relevant property of particulate media is the stress dependent contractive or dilative behavior, which was already understood by Darwin and Reynolds at the end of the 19th century. Dilatency is the tendency of a confined mass to increase volume upon shear; in general, the lower the confinement, the higher the dilative tendency.

Insight into the causal factors that determine macrobehavior can be attained by analyzing particulate media at the particle level. Research on micromechanics has involved both numerical and experimental studies. These studies monitor each particle, including displacement, rotation, contacts, and normal and shear forces at contacts, etc. During the 1980s, micromechanic research emphasized large strain behavior, and was conducted on homogeneous particles, of simple circular geometry. These efforts showed that macrobehavior can be predicted from the statistical characterization of microparameters, such as polar histogram of coordination number, and polar distributions of average normal and tangential contact forces.

Article was reviewed and approved for publication by the Food and Process Engineering Inst. of ASAE in January 1995.

The authors are **M. Aloufi,** Graduate Student, Dept. of Civil Engineering, and **J. C. Santamarina,** Associate Professor, Dept. of Civil Engineering, University of Waterloo, Waterloo, Ontario, Canada.

Rothenburg and co-workers used the micromechanics approach to study the effect of particle slenderness (s = main axis/minor axis) or eccentricity (ecc = [s – 1]/[s + 1]) on the behavior of particulate media (Rothenburg and Bathurst, 1992a, b; Rothenburg, 1993; see also photoelastic study by Oda et al., 1985, and the comprehensive review by Feda, 1982). The main conclusions were:

- Elliptical particles require higher coordination numbers than spherical particles to attain stable configurations (in mathematical terms, the tendency of elliptical particles to rotate implies the additional moment equilibrium equations).
- If two media have the same coordination number, an increase in confining stress will produce a higher increase in coordination number in the medium with higher eccentricity of particles.
- Particle eccentricity magnifies the mechanical anisotropy of a medium subjected to anisotropic loading. This is observed at the level of contact distribution and both normal and tangential contact forces.
- The effect of eccentricity on strength depends on the level of particle slenderness. At low eccentricity, the coordination number increases with respect to spherical particles, and strength increases. However, particles with high eccentricity rotate and become aligned reducing the peak friction angle.

The inherent characteristics of food-grains such as non-linear material behavior, environment sensitive properties, and time dependent creep add further complexity to the mechanical characterization of grain masses (e.g., Mohsenin, 1970; Kocher and Summers, 1988; Li et al., 1990; Hardin et al., 1990).

The goal of the present study is to evaluate the mechanical behavior of three food grains of different eccentricity at low, medium, and large strains, and to analyze results within the framework of micro-mechanical particle interaction in order to gain insight on internal

processes. Measured properties can be used to enhance the design of storage structures and transportation systems (e.g., Jenike, 1966; Diez and Godoy, 1992; Xu et al., 1993), and to develop innovative monitoring techniques based on the propagation of mechanical waves (e.g., Santamarina and Potts, 1994). Grain selection, material properties, and equipment design are discussed next, followed by results and analyses.

Materials and Methods

Three grains of different eccentricity were selected for this study: green peas, white navy beans, and long grain parboiled rice; the three grains were of store quality. Grain size was measured with a micrometer along the three principal directions of the grain. Standard metallurgical hardness tests procedures could not be implemented on grains due to softness and brittleness. The procedure used was designed to provide a reliable measure of the relative hardness of grains. Grains were held in an epoxy bed, and indented with a 1.6-mm-steel spherical tip and the sitting load of an Avery hardness testing machine. The ramp-load history lasted 3 s, reaching a maximum load of 60 N. The diameter of indentations were determined with a calibrated optical microscope.

Devices for small, medium, and large strain testing were used in this study. All devices were large size to minimize scale effects related to the relative size of samples with respect to the size of grains (Bock et al., 1991; see Johnson et al., 1987 for a discussion of shear devices). Large deformation interface behavior was studied in a torsional ring shear. Mid-strain testing was conducted in axi-symmetric and true triaxial devices. Low strain wave propagation properties were determined within the true triaxial and in a large size simple shear device designed and built to study the effect of fabric changes on wave propagation. Samples were prepared within the different test devices by the dry-pluviation technique, raining grains from a constant height h ≈ 0.2 m; followed by light surface tamping. Transducers used in all devices were calibrated following standard procedures. Details are presented next (fig. 1).

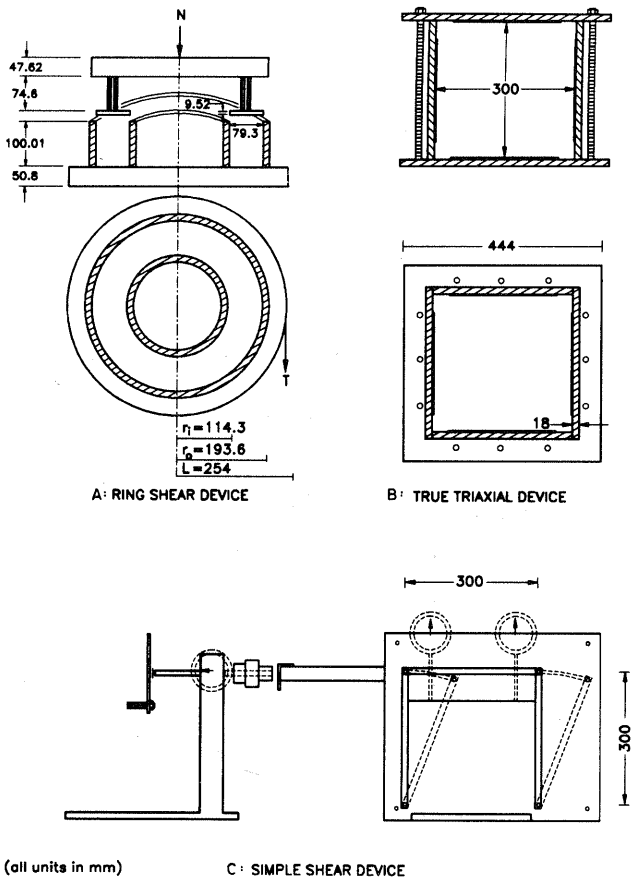

Figure 1–Test devices.

Ring Shear – Interface – Analysis of Fabric

Torsional shear is often preferred to study residual parameters at large strains (ε > 10%). Annular samples reduce the effects of strain gradients along the radius. The ring shear device used in this study was specifically designed to study grain-surface interaction at large strain. It consisted of a U-shaped annular steel container mounted on self aligning vertical and axial bearings (fig. 1a). The annular container had an external radius of r_o = 190 mm, and an internal radius of r_i = 110 mm, thus the annulus width was 80 mm. The loading platen, also of annular shape, fitted into the annular container. Torsion was applied on the lower part of the cell, at a constant rate of deformation. Interchangeable "shoes" could be mounted on the loading platen to study grain-surface interaction. The shoe could be made of materials of different hardness (e.g., wood, steel, or polymers) and roughness (e.g., smooth or rough). Ribbed surfaces were selected to force the failure plane to take place through the grain mass. The steel surface shoe consisted of square teeth, 2 mm deep and 3.6 mm wide, at an average gap width of 2 mm. The applied vertical pressure was 76 kPa. The torsional resistance was computed by integrating the shear resistance on the plane of the annulus, and solving for the mobilized interface friction angle δ_{mob}:

$$\delta_{mob} = \tan^{-1}\left[\frac{3M}{2N}\frac{(r_o^2 - r_i^2)}{(r_o^3 - r_i^3)}\right] \quad (1)$$

where M is the applied torsional moment and N the applied normal force. The rate of deformation imposed in this study was 5 mm/min for the first 100 mm displacement, and then raised to 10 mm/min. Measurements included the tangential force, the rotation of the lower plate, and the vertical movement of the loading annular platen.

After a shear displacement of 400 mm, samples were impregnated with epoxy resin. The resin was injected into the granular material through injection ports, and allowed to set. Once hard, samples were sawed along and across the shear plane, leaving vertical and horizontal planes exposed for analysis. Manual image analysis of the horizontal plane was implemented by identifying the main axis of grains, and measuring their direction with respect to the radial direction. The estimated accuracy of this procedure was ±3° for the elongated rice particles (the radial-normality condition restricted the use of the computerized image

analyzers that were available). More than 150 particles were measured for each type of grain.

Axisymmetric Triaxial

Typical load deformation data and strength parameters were determined using 100-mm-diameter and 200-mm-tall cylindrical samples, following standard axisymmetric triaxial testing procedures. The deformation rate was fixed at 1.0 mm/min. Instrumentation was limited to the monitoring of confining pressure, deviatoric load, and vertical deformation. Samples were tested without fluid saturation to avoid alterations in behavior (under these conditions, no accurate measurements of volume change could be made). The loading path consisted of isotropic loading, followed by axial deviatoric loading.

True Triaxial and Wave Propagation

A large size cubical triaxial was used to characterize the three selected grain masses at mid-strain and low strain levels ($\varepsilon \approx 5 \cdot 10^{-6}$ to $\varepsilon \approx 3\%$). The cubical triaxial cell was 300 mm in width, and it was built out of 12.5-mm-thick aluminum plates (fig. 1b), to withstand 700 kPa pressure.

Six neoprene bladders were internally mounted against the walls; they were inflated and pre-yielded prior to testing so that pressure measurements were not affected by the stiffness of bladders. Opposing bladders were connected together to one of the three ports on the pressure control panel, which allowed independent control of the three principal stresses. The pressure control panel included precision burettes to monitor volume changes (0.1 cm^3). Bladders and all connecting pipes were carefully de-aired to monitor volume changes during loading and unloading. During sample preparation, bladders were collapsed against the walls by applying vacuum through the control panel.

The stress path selected for these tests was isotropic loading to 350 kPa, followed by lateral unloading (constant vertical pressure of 350 kPa), and completed with vertical unloading at constant horizontal pressure. This load path facilitates interpretation and parallels load-relaxation-relief field situations. Strains during loading were computed by dividing volume changes ΔV with the cross-section of the bladder L_o^2, and normalizing with respect to the initial length of the sample, L_o; therefore,

$$\varepsilon_x = \frac{\Delta V_x}{V_o} \qquad (2)$$

The same computation was repeated for directions y and z. It is important to recognize that cubical triaxials have complex boundary conditions (e.g., corners and along edges where normal bladders intersect). Hence, equation 2 gave a first order approximation to the true strains the material was subjected to.

Low strain material properties ($\varepsilon < 10^{-4}$) were obtained from wave propagation measurements that were concurrently performed during true triaxial testing. Three piezocrystal transducers were placed along a vertical line, at the center of the sample; one acted as source and the other two as receivers, minimizing triggering errors. The receiving crystals were mounted at the third-points, and were connected through coaxial cables to a digital storage oscilloscope that was triggered with the source. The velocity of propagation V was obtained by dividing the distance between transducers ΔL by the travel time Δt obtained from the time series. Given the geometry of the sample, measured velocities related to the low strain constrain modulus M of the material (ρ: density of the material):

$$M = V^2 \cdot \rho = \frac{\Delta L^2 \cdot \rho}{\Delta t^2} \qquad (3)$$

Simple Shear and Wave Propagation

Major fabric changes in soft-grained particulate media occur in the strain range between 1% and 10% (to be shown in the sequel). Wave propagation data can be used to study these internal material changes. A large size simple shear box was designed and built to operate to shear strains $\gamma \leq 25\%$, while at the same time allowing for the monitoring of wave propagation in different directions across or within the plane of shear. The simple shear device was 300 mm high, 200 mm wide, and 300 mm long (fig. 1c). Two of the four vertical walls were hinged, and pivoted during shear, while the other two remained normal to the base. The box design included details to reduce boundary effects, and to minimize reflected and refracted waves. The three grain masses were tested in this device, at the relatively low normal stress of 15.1 kPa, compatible with equipment design.

The instrumentation consisted of transducers to measure shear load, shear deformation, dilatency, and normal force against the two parallel fixed walls. A needle pulse source acted through the upper platen, and was activated with a pulse generator. Thin piezocrystal transducers ($t \approx 0.1$ mm) were placed on the lower plate to monitor the arrival of transmitted waves. The source and receivers were vertically oriented on the central plane of the simple shear device. The relative location of source and receivers allowed for different directions of the assumed ray paths.

Results and Discussion

Index Properties

Measured index properties included grain size, eccentricity, unit weight of particles, and minimum and maximum void ratio. Results are summarized in table 1. The slenderness of rice is larger than the slenderness of navy beans and green peas. Green peas are the most spherical of the three. The three tested grains differ not only in geometrical but also mechanical characteristics. Hardness data presented in table 1 show that rice grains are harder than navy beans, which are harder than green peas. Microscopic observation emphasized the higher surface roughness in rice than in green peas and navy beans. Differences in index properties are statistically significant. Mechanical and geometrical properties couple to affect macrobehavior, making test interpretation cumbersome.

When spherical monosized particles are placed in a container, and allowed to attain stable arrangements corresponding to a minimum potential energy, the void ratio of these random assemblies is usually between well defined bounds, corresponding to the loose and dense

Table 1. Summary of Results

Parameter*	Green Peas	Navy Beans	Rice
Size – Slenderness			
L1 (50) [mm]	7.02±0.34†	7.74±0.52†	6.62±0.59†
L2 (50) [mm]	6.31±0.35†	5.90±0.34†	1.95±0.19†
L3 (50) [mm]	5.80±0.55†	5.09±0.35†	1.34±0.14†
s = L1/L3 [ ]	1.21	1.52	4.94
ecc = (s – 1)/(s + 1) [ ]	0.09	0.21	0.66
Hardness (10)			
diameter indentation [mm]	1.28±0.07	1.06±0.04	0.78±0.07
Unit weight of grains (3) [kN/m^3]	13.05	13.44	13.93
Gravimetric moisture content [%]	7.1	7.3	8.0
Maximum void ratio (3) [ ]	0.64	0.67	0.88
Minimum void ratio (3) [ ]	0.59	0.58	0.65
Low-strain: Wave propagation			
α (at 100 kPa) [m/s]	366	333	274
β [ ]	0.44	0.37	0.17
Structural change [strain]	gradual	<8%	<4%
Mid-strain bulk modulus			
B at σ = 100 kPa	4380	4680	9210
Angle of internal shear resistance			
Triaxial Testing			
ϕ peak (0-100 kPa) [deg]	30	27	35
ϕ peak (100-300 kPa) [deg]	24	26	27
Relative density	dense	dense	dense
Failure mode	bulging	banding	bulging
Large strain interface resistance			
δ (76 kPa) [deg]	23	24.5	24
Relative density	dense	dense	dense
Post failure fabric	–	–	part. align.

* (#) = Number of measurements.
[unit] = Dimensions of the measurement.
† Mean ± standard deviation.

random packing. Scott et al. (1964) showed that these extreme void ratios range between 0.570 and 0.664 for the dense and loose packing of spherical monosize particles (see also the classical work by Graton and Fraser, 1935). On the other hand, particle eccentricity induces particle rotation and alters the random packing of slender particles. Data in Shinohara (1984) show that the higher the slenderness of particles, the higher the porosity, yet the lower the range between lose and dense packing; in addition, the higher the roughness of particle surfaces the higher the porosity. Trends for minimum and maximum void ratios for the three selected grains are in agreement with Scott et al. (1964) and Shinohara (1984). The dry-pluviation method for sample preparation produces dense samples. Preferential grain orientation is visually observable in rice samples after pluviation, where the main axis of grains is on the horizontal plane, yet in random orientation. These are among the earlier consequences of particle eccentricity on the macro characteristics of the medium.

Large Strain Interface Behavior

Characteristic ring shear test results are presented in figure 2. The three materials show similar response: the deformation required to yield the interface strength is between 8 mm and 10 mm, and the interfacial friction is about 24°. This similarity in behavior is striking, given the marked differences in the geometrical and mechanical properties of the selected grains (see also triaxial strength data in the sequel). Unfortunately, the rotation of principal stresses at the interface hinders further mechanical interpretation of this test.

To further assess the effect of interface properties on interface behavior, a second toothed shoe was tested, but with the inverse teeth geometry: gap width was 4.7 mm and average tooth width was 12 mm. While green peas and navy beans produced results similar to those presented in figure 2, rice showed very different trends: multiple peaks were observed during the first 100 mm displacement, and a large deformation post-peak behavior was incipient after 250 mm displacement, with decreasing strength. Differences in the results for rice highlight the influence of interface geometry on grain-surface interaction, at least in this case where the scale of surface features approaches the grain size.

The vertical plane in resign-impregnated samples shows the thickness of the shear band along which shear took

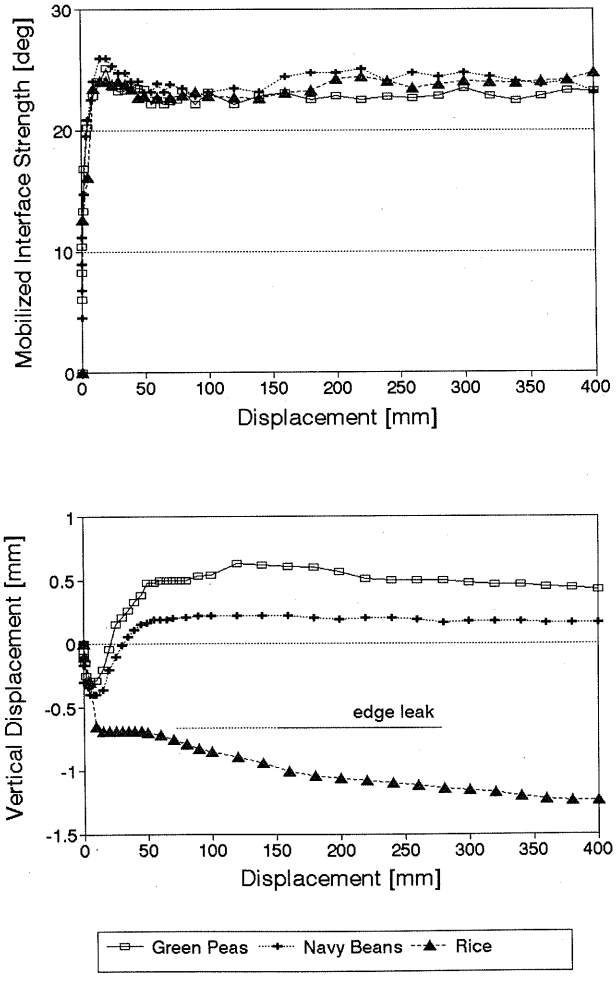

Figure 2–Torsional ring shear – large strain interfacial behavior.

place. This region is most noticeable for rice, reaching a depth of approximately 10 mm; the alignment of rice grains on the vertical tangential plane is not flat (parallel to the shearing surface), but reveals a preferential tilt of 24° ± 5° with the horizontal, so that the main axis of rice grains is rotated towards the minimum principal stress.

Results of manual image analysis of grain orientation on the horizontal plane are presented in figure 3. The alignment of semi-spherical green peas and navy beans was minimum and is probably biased by the measurement method and the lack of clear main axis; however, rice shows strong preferential orientation. The polar histogram of particle orientations is well approximated by a second-order Fourier series, with no apparent advantages of higher order terms (note that due to particle alignment on the vertical plane, the horizontal plane is not the plane of maximum particle alignment anisotropy).

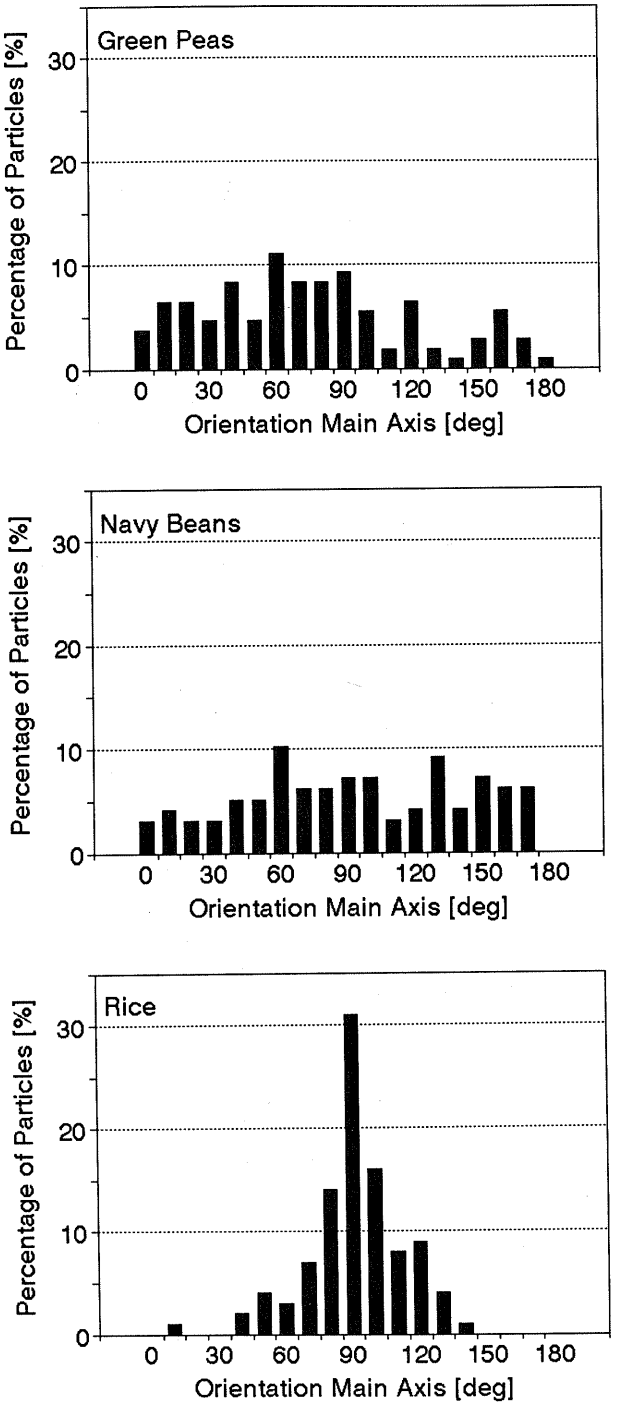

Figure 3–Orientation of main axis after large strain torsional testing.

Mid-strain Parameters – Axisymmetric Triaxial

During deformation controlled loading, frequent and sudden drops in load were observed; these "slips" were most noticeable in green peas and least significant in rice. Stable load values were recorded. Load deformation data are presented in figure 4, and strength parameters are summarized in table 1. The following observations can be made: (1) the curvature of the failure envelope is least pronounced for navy beans, (2) green peas and navy beans do not show post-peak behavior even at low confinement, (3) green peas samples bulge and do not present a clear

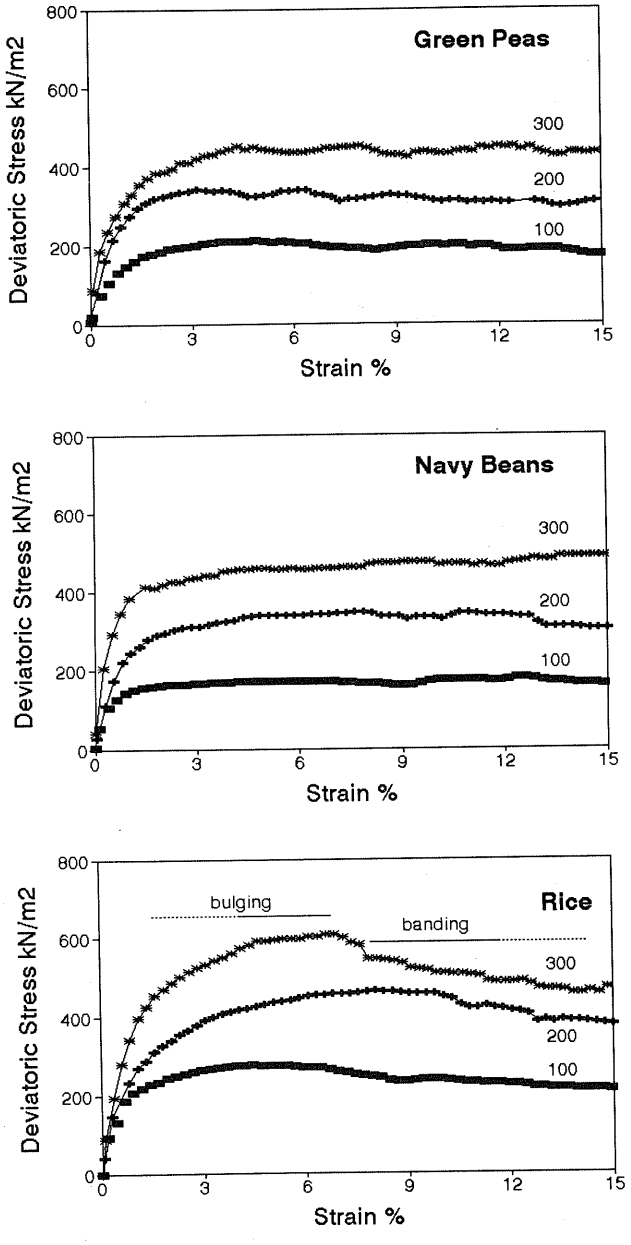

Figure 4–Axisymmetric triaxial test data – axial compression (numbers indicate confining pressure in kPa).

failure plane; rice and navy beans bulge until the peak load and then produce very clear strain localization along a main shear band, and (4) rice exhibits highest post peak behavior at high confinement, even though high confining stress accentuates strain hardening behavior in typical particulate materials.

Four additional rice samples were tested to verify these observations: the variability in strength can reach 4° for individual samples, probably as a result of differences in initial fabric; all data confirms that post-peak softening increases with confinement (the loss in strength was sudden in two samples tested at 300 kPa confining pressure); and extensive particle alignment develops along very well defined failure planes in all samples. Apparently, destructuring of the material and major changes in fabric occur within localized regions, the medium loses its strength and deforms along shear bands.

A simplified two-dimensional analysis is attempted to evaluate the consequences of particle eccentricity and large strain alignment. Let's consider an elliptical particle centrally located on top of two identical elliptical particles (fig. 5). Evaluation of the dilatency angle involved in sliding the top particle pass the lower two, leads to the following relationship between the angle of dilatency i and slenderness (fig. 5):

$$\tan(i) = \frac{b}{a} \tan\left(\frac{\pi}{6}\right) \qquad (4)$$

This equation is plotted in figure 5. Slenderness b/a > 1 implies particle alignment normal to the shearing direction, and resembles the situation of the horizontally aligned rice particles during early vertical deviatoric loading. On the other hand, b/a > 1 indicates alignment parallel to shear; this is the case of rice particles along the shear plane at large deformation. The change in dilatency between normal and parallel alignment explains the high early strength of rice and the post-peak strength loss. The higher post peak loss with increased confinement may reflect the contribution of the Colombian interparticle friction restraining particle rotation.

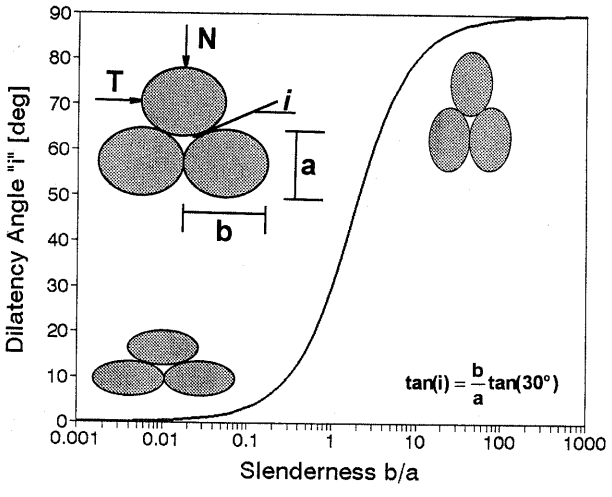

Figure 5–Slenderness, alignment, and dilatency.

This analysis also shows that the residual angle of internal shear resistance, ϕ, decreases as the slenderness of particles increases, other factors being constant. It is known that even loose contractive clays present post-peak behavior at large strain due to the alignment of particles along the shear plane; in the case of clays, the residual effective friction angle can be as low as 3° or 4° along specular surfaces (e.g., Lambe and Whitman, 1969).

This three-particle analysis does not take into consideration rotational freedom (hence it cannot predict particle tilt on the vertical plane), and simplifies the complexity of interactions and compensations taking place within the grain mass (e.g., dilatency is overpredicted). However, it is a first order material model that facilitates assessing the interactions among particles, and between particles and interfaces.

Mid-strain Parameters – True Triaxial

Results are presented in figure 6. It can be seen that rice mass is stiffer than navy beans and green peas. For the maximum isotropic load of 350 kPa the deformation due to compression does not exceed 3% in rice, while it reaches 6.5 and 7.7% in green peas and navy beans, respectively. Residual volumetric deformations after unloading are 2.5% for rice, 5% for green peas, and 7% for navy beans (unloading continued until volumetric changes indicated proximity to failure). Figure 6 also presents the strains in x, y, and z versus the volumetric strain. Rice, which is the least spherical of the three selected grains and the one with initial fabric anisotropy, displays isotropic strains not only in the horizontal plane but also in the vertical direction during isotropic loading.

Volume changes reflect (1) particle re-accommodation, which is enhanced by particle eccentricity, and (2) deformation of particles which depends on their elasto-plastic behavior. The second mechanism is expected to prevail under isotropic loading. Even though rice has a higher ability to rotate and reaccommodate, the higher bulk modulus B observed in figure 6 (table 1) points to the significantly lower deformability of rice grains compared to the other two grains. This agrees with hardness data shown in table 1.

Velocity of Propagation – True Triaxial

There are many implications from low strain, wave propagation data. For example, if wave propagation velocities are clearly related to the state of the stress, then wave propagation measurements may be used to monitor stress, and changes in stress. These data are also needed for constitutive equations used in numerical modeling.

Wave velocities determined in the true triaxial device varied during the first few minutes after each load change (i.e., viscous contact behavior); all reported measurements were obtained 10 min after load application. Figure 7 shows computed velocities versus the stress in the direction of propagation, during (a) isotropic loading, (b) lateral unloading, and (c) final vertical unloading.

The velocity of propagation of P-waves in particulate media is related to the stress in the direction of propagation, which is the same as the direction of particle motion. The relationship between the velocity of P-waves, V_p, and the stress acting in the direction of propagation, σ_{prop}, follows a power relation (Roesler, 1979):

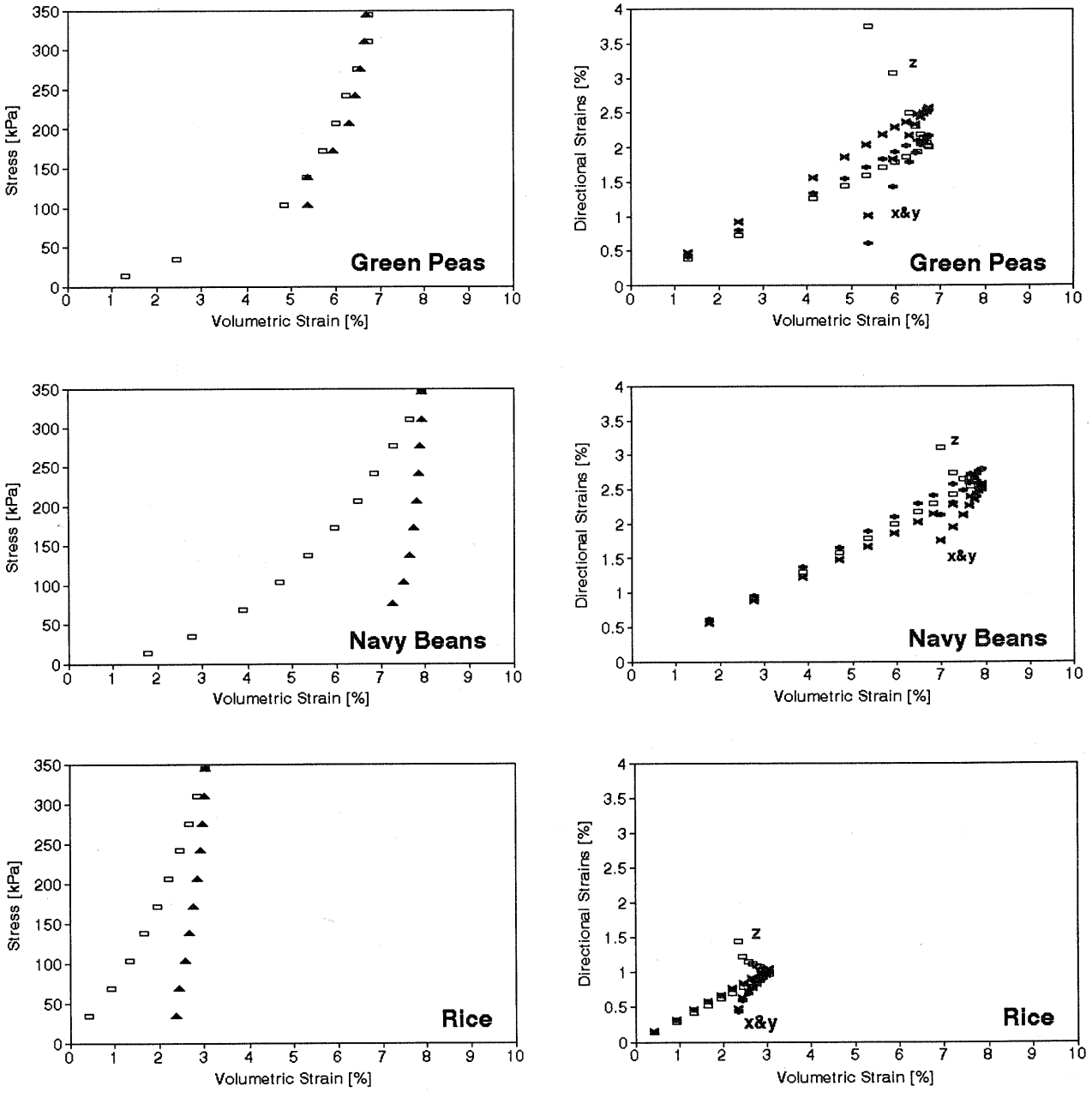

Figure 6–True triaxial – mid-strain testing.

$$V_P = \alpha \cdot \left(\frac{\sigma_{prop}}{1 \cdot atm}\right)^{\beta} \qquad (5)$$

where α and β are constants. This equation is equivalent to the relationship between low strain modulus versus stress used in Hardin et al. (1990) and Li et al. (1990). Data in figure 7 are plotted in log-log scale to facilitate assessing the validity of the power relationship proposed above.

In the case of isotropic loading (fig. 7a), equation 5 adequately fits observed behavior. Linear regressions were computed to obtain stress exponents for the different materials. Results are summarized in table 1. Resonant column tests on wheat by Hardin et al. (1990) exhibit exponents between $\beta = 0.205$ and $\beta = 0.260$ for moisture contents that range between 18 and 8%, respectively (in this case β relates shear wave velocity, V_s, to isotropic confining stresses).

Lateral unloading (fig. 7b), produces no changes in P-wave velocity of rice in the vertical direction. This is in agreement with equation 5 which predicts that the vertical P-wave velocity is only related to the vertical stress, hence, unaffected by horizontal stresses. The changes in velocity during lateral unloading for green peas and navy beans deviate from the observed behavior in hard-grain particulate media, reflecting the effects of soft, plastic grains in macro behavior.

Figure 7c displays the variation of P-wave velocity during the final vertical unloading (stress in z-direction decreases while the stress in directions x and y remains constant). Observed changes are smaller than those measured during the loading stage. This indicates that

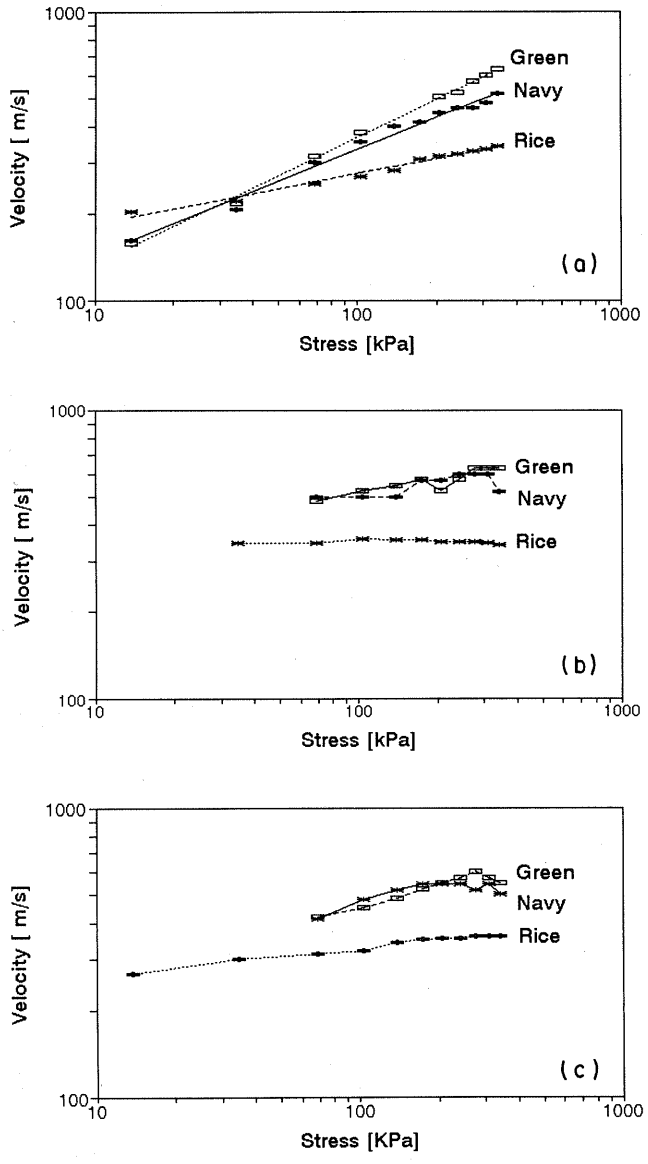

Figure 7–Wave propagation in true triaxial – low strain. (a) Isotropic loading, (b) lateral unloading, and (c) vertical unloading.

prestraining affected fabric and contacts in the particulate medium. Yielded contacts have limited recovery during unloading, hence there will be limited stiffness and velocity changes. Once again, rice shows typical hard-grain behavior.

Hertz' theory predicts that the stiffness of a particulate medium is related to the state of stress to an exponent 1/3 (White, 1983). The velocity of P-waves when $\lambda/D_{50}>>2$ is estimated as:

$$V_P = \sqrt{\frac{M}{\rho}} \qquad (6)$$

where M is the constraint modulus and ρ is the mass density. Then, it follows from Hertz' theory and equation 6 that β should be about 1/6 for monosized spheres made of elastic materials. When the geometry of contacts approaches a cone-to-plane condition, this exponent can be as high as 0.25. The β exponent for rice is in agreement with these values, however, the high values for β obtained for green peas and navy beans require further interpretation. First, it is important to realize that the combination of Hertz' theory and equation 6 presumes constant fabric, however, fabric is modified whenever confinement is changed such as in triaxial testing. Hence, the β-coefficient not only reflects changes in contact stiffness during loading but also changes in fabric. Therefore, one would expect that the lower the mid-strain stiffness of a medium, the higher the fabric changes that take place during loading, and the more relevant the influence on β (Hryciw and Thomann, 1994).

A second concurrent phenomenon that affects β is the viscous-plastic deformation of contacts. Materials that yield produce higher rate of contact flattening upon early loading than elastic materials. This results in higher values of β at low confinement, tending to $\beta = 0$ for high confinement. Ongoing studies within our group, using lead-shots, have confirmed this observation and the time-dependency of the β-coefficient. Contact yield and creep are believed to prevail over fabric changes during the isotropic loading of the samples.

Velocity of Propagation – Simple Shear

To further understand variations in wave propagation during shear, the three grain masses were tested in simple shear (constant normal stress 15.1 kPa). Figure 8 presents the evolution of wave velocity with shear strain for three different ray directions (vertical, 0.3 horizontal to 1 vertical, and 0.5 horizontal to 1 vertical). It is observed that wave velocity decreases more severely for rays that are inclined against the shearing direction. The velocity of wave propagation in rice has an important reduction for strains lower than 4% shear strain, and the velocity drop is most severe in the direction of the rotated minor principal stress. On the other hand, navy beans and green beans present very limited velocity losses, even in the oblique direction, and the drop takes place gradually with shear strain, starting at approximately $\gamma = 4\%$ and extending to strains in the order of $\gamma = 10\%$.

The drop in velocity observed during simple shear in figure 8 is analyzed first with a continuum mechanics approach. Consider the case of a differential element within the simple shear device; then, the addition of shear stress τ_{app} produces an enlarged concentric Mohr circle. Figure 9 presents polar diagrams of normal and shear stress for such an element at initial no-lateral strain condition, i.e., ko-condition, and after shear. It is assumed that the horizontal stress remains constant during simple shear; in reality the stress field is quite complex. Given that ko can be estimated as $ko \approx 1\text{-}\sin\phi$, figure 9a corresponds to $\phi = 37°$ (ko = 0.4), and figure 9b to $\phi = 23°$ (ko = 0.6). These are bounding values for the grains tested in this study.

Results from figure 9, equation 5, and material parameters summarized in table 1 are used to estimate wave velocities for the three materials in different directions, at initial ko-condition, and at failure. Figure 10 presents measured velocities on the left and computed velocities on the right. Velocities in rice change drastically from the initial ko-state to the final state of stress at failure, clearly deviating from predicted trends; changes in navy beans deviate to a lesser extent. These results highlight eccentricity effects on the development of fabric anisotropy

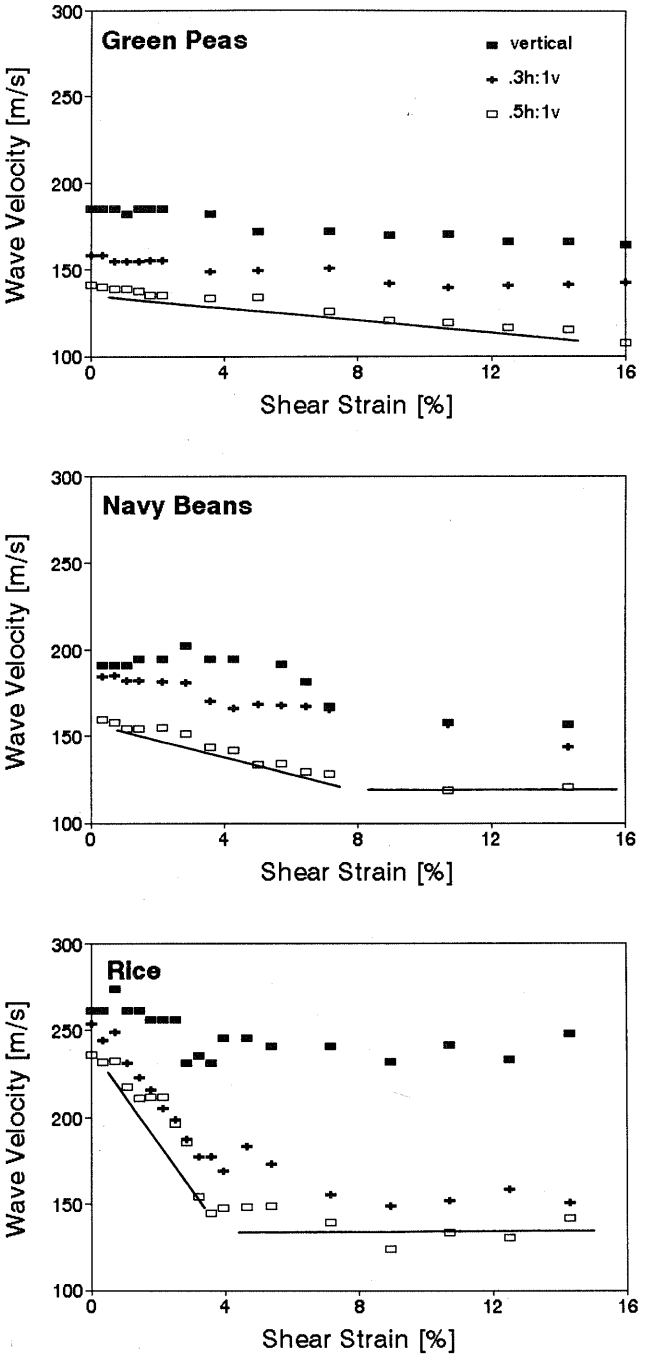

Figure 8–Wave propagation during simple shear. Different directions.

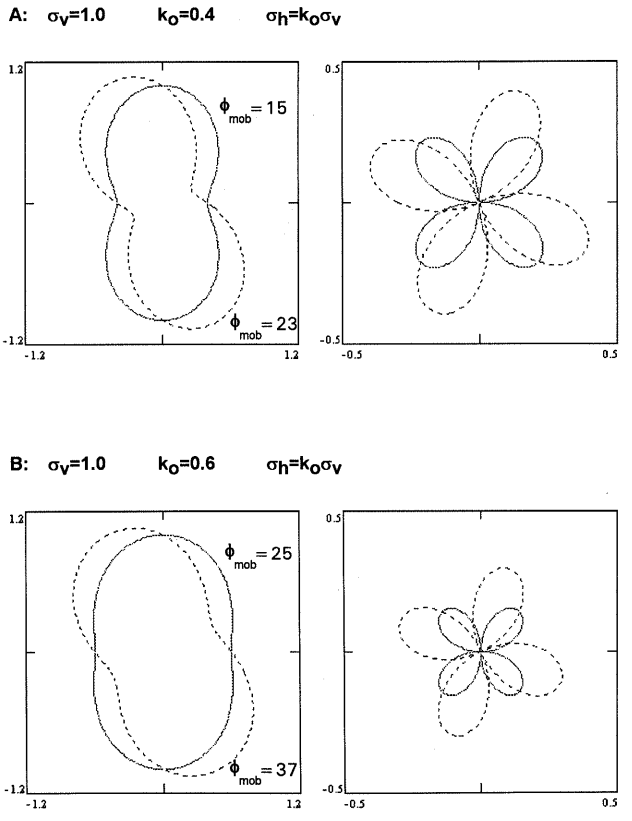

Figure 9–Polar diagram of normal and shear stress during shear (equilibrium – continuum mechanics).

during shear. Furthermore, they promote the reassessment of simple stress-velocity equations, such as equation 5, for such materials and for nonprincipal stress directions.

Results in figure 8 showed that velocity changes occurred at different strain levels in the different grains. To gain insight into this effect, the following micro-scale analysis is proposed. Consider a spherical particle supported on two identical particles, such that their centers define an equilateral triangle (similar to the scheme in fig. 5). An increase in shear force T on the top disk will eventually lead to contact loss in the direction oblique to the shearing direction, increasing the possibility of shear deformation-slippage on the remaining contacts, i.e., lower stiffness, lower velocity, and higher attenuation along the minor principal direction. Force equilibrium analysis shows that the normal contact force doubles in the direction of the shear load when the contact in the oblique direction is lost. Assuming a Hertzian contact law, the horizontal displacement required for contact loss Δ_{loss} is (Aloufi et al., 1993):

$$\Delta_{loss} = \frac{6.4}{d}\left[\frac{3(1-\upsilon)}{8G}\left(\frac{N}{2}\frac{1}{\cos(30)}\right)\frac{d}{2}\right]^{\frac{2}{3}} \qquad (7)$$

where

- υ = Poison's ratio
- G = shear modulus of the material of the grains
- N = the applied normal force on the top grain
- d = the diameter of the grains

This relationship indicates that the lower the normal load applied to the grain mass, and the higher the stiffness of the material of the particles, the lower the shear strain required for contact loss. Indeed, stiff rice particles undergo definite fabric changes at low strains (fig. 8).

CONCLUSIONS

Green peas, navy beans, and rice were tested to assess the effect of particle eccentricity on macrobehavior. Rice grains are the most slender and also the hardest, followed by navy beans. Geometrical and mechanical properties

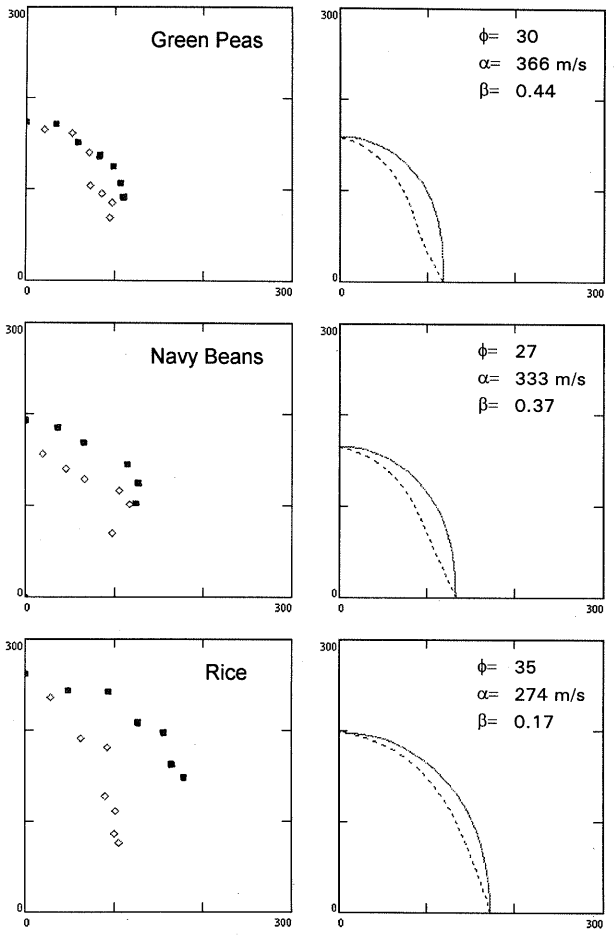

Figure 10–Comparison of measured and predicted velocities (squares and continuous line – before shear and diamonds; dashed line – after shear).

couple, making the interpretation of results more difficult. The interpretation of ring shear and simple shear is hindered by the rotation of principal stresses.

The development of fabric anisotropy at large strain is accentuated by the eccentricity of particles. Rice particles developed distinct anisotropy in particle orientation on the plane of shear; furthermore, preferential particle alignment was observed on the vertical plane, whereby the main axis of particles tilted in the direction of the minor principal stress.

The increase in confinement in axisymmetric triaxial testing enhanced the post-peak behavior of rice, and the tendency for strain localization along shear bands both in rice and in navy beans.

Low strain testing in true triaxial revealed the high sensitivity of the softer green peas and navy beans to the state of stress. This sensitivity is higher than predicted by classical Hertzian theory for elastic spherical contacts at constant fabric. It reflects the viscous-plastic nature of food grain contacts and the changes in fabric.

The development of velocity anisotropy is primarily affected by the changes in contact distribution. The strain required for notable microfabric changes increases for softer materials.

Interfacial behavior was similar for the three grains. Strength reached approximately 24 to 26 after a yield deformation of 10 mm. The characteristics of the boundary have a strong effect of the observed interfacial behavior.

ACKNOWLEDGMENTS. This study is part of a research program on wave-material interaction and applications. K. Bowman helped in the design and construction of test devices. M. Y. Su conducted the true-triaxial tests. The authors are grateful to the reviewers for helpful comments and suggestions. This study was supported in part by Natural Science and Engineering Research Council of Canada.

REFERENCES

Aloufi, M. A., N. T. Huynh and J. C. Santamarina. 1993. Mechanical waves through discrete media, geophysical techniques for dite and material characterization. NSF. *Workshop on the Application of Geophysical Techniques in Civil Engineering*, 115-119. Atlanta, Ga.

Bock, R. G., V. M. Puri and H. B. Manbeck. 1991. Triaxial test sample size effect on stress relaxation of wheat *en masse*. *Transactions of the ASAE* 34(3):966-971.

Diez, M. A. and L. A. Godoy. 1992. Viscoplastic incompressible flow of frictional-cohesive solids. *Int. J. of Mech. Sci.* 34(5):395-408.

Feda, J. 1982. *Mechanics of Particulate Materials*. New York: Elsevier.

Graton, L. C. and H. J. Fraser. 1935. Systematic packing of spheres with particular relation to porosity and permeability, *J. of Geol.* 43(8):785-909.

Hardin, B. O., K. O. Hardin, I. J. Ross and C. V. Schwab. 1990. Triaxial compression, simple shear, and strength of wheat *en masse*. *Transactions of the ASAE* 33(3):933-942.

Hryciw, R. D. and T. G. Thomann. 1994. A compressibility-based model for the elastic shear modulus of cohesionless soils. *ASCE J. of Geotech. Eng.* (In press).

Jenike, A. W. 1966. Storage and flow of solids. Utah Engineering Experiment Station, Bulletin 123.

Johnson, C. E., R. D. Grisso, T. A. Nichols and A. C. Bailey. 1987. Shear measurement for agricultural soils – A review. *Transactions of the ASAE* 30(4):935-938.

Kocher, M. F. and J. D. Summers. 1988. Wave propagation theory for evaluating dynamic soil stress-strain models. *Transactions of the ASAE* 31(3):683-691.

Lambe, T. W. and R. V. Whitman. 1969. *Soil Mechanics*. New York: John Wiley.

Li, Y., V. M. Puri and H. B. Manbeck. 1990. Elastic-viscoplastic cyclic constitutive model parameter determination and evaluation for wheat *en masse*. *Transactions of the ASAE* 33(6):984-995.

Mohsenin, N. N. 1970. *Physical Properties of Plant and Animal Materials*, Vol. 1. New York: Gordon and Breach Science Publishers.

Oda, M., S. Nemat-Nasser and J. Konishi. 1985. Stress-induced anisotropy in granular masses. *Soil and Foundation* 25(3):85-97.

Richart, F. E., J. R. Hall and R. D. Woods. 1970. *Vibrations of Soils and Foundations*. Englewood Cliffs, N.J.: Prentice-Hall.

Roesler, S. K. 1979. Anisotropic shear modulus due to stress anisotropy. *J. of the Geotech. Eng. Div., ASCE* 105(GT7):871-880.

Rothenburg, L. 1993. Effects of particle shape and creep in contacts on micromechanical behavior of simulated sintered granular media. Dept. of Civil Engineering, Univ. of Waterloo, Waterloo, Ontario, Canada.

Rothenburg, L. and R. J. Bathurst. 1992a. Effects of particle shape on micromechanical behavior of granular materials. In *Advances in Micromechanics of Granular Materials,* eds. H. H. Shen, M. Satake, M. M. Mehrabadi, C. S. Chang and C. S. Campbell. Amsterdam: Elsevier.

————. 1992b. Micromechanical features of granular assemblies with planar elliptical particles. *Geotechnique* 42(1):79-95.

Santamarina J. C. and B. Potts. 1994. Tomographic imaging stress changes in granular media. An experimental study. *Canadian Geotechnical J.* 31(2):215-222.

Scott, G. D., A. M. Charlesworth and M. K. Mak. 1964. On the random packing of Spheres. *J. of Chem. Physics* 40:611-612.

Shinohara, K. 1984. Fundamental properties of powders. In *Handbook of Powder Science and Technology,* eds. M. E. Fayed and L. Otten. New York: Van Nostrand Reinhold.

White, J. E. 1983. Some model of earth materials. *Underground Sound.* New York: Elsevier.

Xu, S., Q. Zhang and M. G. Britton. 1993. An endochronic finite element model for predicting loads in grain storage structures. *Transactions of the ASAE* 36(4):1191-1199.